A numerical analysis of dimensionality and heterogeneity effects on advective dispersive seawater intrusion processes

Jaouher Kerrou · Philippe Renard

Abstract Two-dimensional (2D) and 3D numerical simulations of the dispersive Henry problem show that heterogeneity affects seawater intrusion differently in 2D and 3D. When the variance of a multi-Gaussian isotropic hydraulic conductivity field increases, the penetration of the saltwater wedge decreases in 2D while it increases in 3D. This is due to the combined influence of advective and dispersive processes which are affected differently by heterogeneity and problem dimensionality. First, the equivalent hydraulic conductivity controls the mean head gradient and therefore the position of the wedge. For an isotropic medium, increasing the variance increases the equivalent conductivity in 3D but not in 2D. Second, the macrodispersion controls the rotation of the saltwater wedge by affecting the magnitude of the density contrasts along the saltwater wedge. An increased dispersion due to heterogeneity leads to a decreasing density contrast and therefore a smaller penetration of the wedge. The relative magnitude of these two opposite effects depends on the degree of heterogeneity, anisotropy of the medium, and dimension. Investigating these effects in 3D is very heavy numerically; as an alternative, one can simulate 2D heterogeneous media that approximate the behaviour of the 3D ones, provided that their statistical distribution is rescaled.

Keywords Heterogeneity · Seawater intrusion · Monte Carlo simulations · Effective parameters · Salt-water/fresh-water relations

Received: 15 December 2008 / Accepted: 13 September 2009
Published online: 13 November 2009

J. Kerrou (✉) · P. Renard
Centre for Hydrogeology,
University of Neuchâtel,
Rue Emile Argand, 11 - CP158, 2009, Neuchâtel, Switzerland
e-mail: jaouher.kerrou@unine.ch
Tel.: +41-32-7182602
Fax: +41-32-7182603

P. Renard
e-mail: philippe.renard@unine.ch

Introduction

In most coastal aquifers, the excess of freshwater flows toward the sea. However, near the shoreline, heavier seawater penetrates inland underneath freshwater due to density-driven flows and forms a mixing zone between the two fluids. Under natural conditions, the geometry of the saltwater wedge depends on the hydraulic properties of the aquifer, on the physical properties of the two fluids (e.g. Glover 1959; Henry 1964; Voss and Souza 1987; Croucher and O'Sullivan 1995), on the aquifer geometry (e.g. Abarca et al. 2007b), and/or on the tidal patterns (e.g. Brovelli et al. 2007). The geometry and extension of the saltwater wedge depends also on the degree of heterogeneity of the aquifer (e.g. Dagan and Zeitoun 1998; Held et al. 2005).

To simulate the seawater intrusion (SWI), one can either adopt a sharp interface or a density-dependent dispersive model (Bear 2005). The sharp interface approach was introduced by Badon-Ghyben (1888) and Herzberg (1901). The freshwater and saltwater are considered immiscible. This simplification allows for treatment of the problem analytically (Glover 1959; Dagan and Bear 1968; Fetter 1972; Strack 1976) or numerically (Huyakorn et al. 1996) in a very efficient manner. Reviews of this approach can be found in Reilly and Goodman (1985) or Bear (1999). Despite the fact that assuming a sharp interface allows the development of solutions that are useful for understanding SWI and for solving real-world problems, this approach does not account for hydrodynamic dispersion. However, it is well known that instead of a sharp interface between freshwater and saltwater there is a transition zone since both fluids are miscible (Henry 1964). Therefore several methods have been developed to solve the coupled variable-density flow and advective-dispersive solute transport equations. These methods were reviewed by Simmons et al. (2001) and Diersch and Kolditz (2002), who stated that one of the major challenges in SWI modelling using both sharp interface or density dependent dispersive transport is to account for spatial heterogeneity.

In the case of unstable variable density flow and transport, Simmons et al. (2001) have shown that heterogeneity can affect transport over many length scales. In the case of stable SWI, Dagan and Zeitoun (1998) studied the effect of a layered one-dimensional (1D) heterogeneity on a 2D vertical section assuming a sharp

 DOI 10.1007/s10040-009-0533-0

interface model. Al-Bitar and Ababou (2005) also used a sharp interface model to investigate on a 2D horizontal section the impact of a multi-Gaussian heterogeneity on SWI. They developed an analytical expression for the first two moments of the position of the interface and compared it with the results of a numerical model. Another group of authors (Schwarz 1999; Darvini et al. 2002; Held et al. 2005; Abarca 2006) investigated the effects of heterogeneity of hydraulic conductivity on 2D vertical sections inspired by the Henry problem (1964). Held et al. (2005) used homogenization theory to derive expressions for the effective hydraulic conductivity and dispersivities in 2D isotropic and anisotropic heterogeneous permeability fields. They showed that for an isotropic heterogeneous medium whose small scale (local) log permeabilities follow a multi-Gaussian statistical distribution, the effective permeability corresponds to the geometric mean of the local permeabilities. This finding is in agreement with the theoretical effective conductivity for log multi-Gaussian fields under uniform flow conditions and constant fluid density (Matheron 1967). For an anisotropic medium, the expression derived by Held et al. (2005) is identical to that of Gelhar (1993) for the case without density effects. In addition, Held et al. (2005) showed that the dispersion coefficients that should be used to model SWI in an equivalent homogeneous medium correspond to the local dispersion coefficients rather than the macroscopic coefficients. In other words, according to the results of Held et al. (2005), it is not necessary to upscale the dispersivity coefficient to reproduce accurately the mean behaviour of the SWI wedge in a heterogeneous medium. More generally, the behaviour of the SWI as a function of the degree of heterogeneity of the medium has been well described in 2D by Held et al. (2005) or Abarca (2006). One aim of the present paper is to investigate whether these results are also applicable in 3D.

Related to the question of heterogeneity, one has also to consider the problem of dimensionality when modelling seawater intrusion in a heterogeneous aquifer. Indeed, it is common practice to model groundwater flow and transport problems in 2D or 1D because of limited computing resources even if the real problem is 3D. When the reality is assumed homogeneous, exact results can be obtained with a reduced dimension if the appropriate boundary conditions and model size are taken into account. However, this is not sufficient when heterogeneity has to be considered. The choice of dimensionality can lead to significant differences in the outputs of the models (Gelhar and Axness 1983). Burnett and Frind (1987) pointed out such effects on transport model predictions (without density variation) when reducing a 3D system to a 2D one. They showed that the simulated plume advances farther in a 2D vertical cross-section than in the reference 3D plume simulation. They also showed that vertical averaging of a 3D system would not give sufficiently correct predictions in the case of a vertically extensive plume. Shapiro and Cvetkovic (1990) also compared 2D and 3D interpretations of stochastic solute transport in porous media without density effects. They showed that the longitudinal and transversal dispersion of the solute plume is underestimated in the case of a 2D simulation (vertical averaging of 3D hydraulic conductivity field). Pohll et al. (2000) investigated the error associated with a 2D model for the simulation of solute breakthrough. They found that the removal of the vertical dimension and its hydraulic conductivity variability introduces a 5–10% underestimation of the solute velocities. Given the findings of previous studies, it is expected that dimensionality also affects the result of density-dependent flow and transport models. That is why this paper investigates jointly the effects of heterogeneity and problem dimensionality on density-dependent SWI.

The research is conducted using numerical modelling and Monte Carlo simulations. The conceptual framework follows previous works on the effect of heterogeneity on 2D density dependent problems (Held et al. 2005; Abarca 2006; Abarca et al. 2007a) and is extended in 3D. The heterogeneity is modelled with a multi-Gaussian approach and considers isotropic and anisotropic media. This approach allows for investigation of the progressive transition from a 3D medium (finite correlation lengths in the three directions) to a 2D medium (infinite correlation along the sea shore). Varying the variance of the log hydraulic conductivity allows one to study the effect of increasing level of heterogeneity. Systematic Monte Carlo simulations are then used to investigate the behaviour of the SWI in heterogeneous media. The effective hydraulic conductivities of the 2D and 3D media are estimated using standard upscaling techniques, and the SWI in the homogeneous media is computed too. The analysis of these results show that different behaviours (even sometime opposite) can be observed when comparing the evolution of the saltwater wedge position as a function of increasing levels of heterogeneity in 2D and 3D configurations. These results indicate that previous observations (e.g. Abarca 2006; Held et al. 2005) were valid only for the 2D case and cannot be directly extended in 3D. In addition, the results obtained on heterogeneous and homogeneous models sharing the same effective hydraulic conductivities are compared. They show that an upscaling of the dispersivity is required if one wants to reproduce the mean behaviour of a heterogeneous field by an effective medium. This contradicts previous findings from Held et al. (2005). From a more practical point of view, the results suggest that it is possible to approximate SWI in a 3D heterogeneous field by using an equivalent 2D vertical heterogeneous medium. The main advantage of the proposed approximation is that it offers a fast and reasonably accurate approximation that one can use for real case applications avoiding the need to conduct large and time consuming 3D simulations.

Problem setup

The SWI conceptual model

Abarca et al. (2007a) modified the Henry problem (1964) to set up an anisotropic dispersive version of it. The

 DOI 10.1007/s10040-009-0533-0

fundamental modification is the assumption that mixing between freshwater and saltwater results from advection and velocity-dependent dispersion processes rather than advection and pure diffusion. The second modification is the use of an anisotropic hydraulic conductivity tensor instead of an isotropic one. These modifications lead to a more realistic simulation of seawater intrusion phenomena, especially more realistic salinity profiles. Abarca et al. (2007a) tested the sensitivity of the mixing zone (length and width) as well as the inflowing seawater to the new model parameters (including dispersion and anisotropy of hydraulic conductivity) and showed that in the dispersive version of the Henry problem, the penetration length depends mainly on the horizontal hydraulic conductivity and the geometric mean of the longitudinal and transversal dispersivities. The width of the mixing zone is controlled by the geometric mean of the longitudinal and transversal dispersivities. Furthermore, the flux of inflowing seawater is controlled by the transverse dispersivity and the geometric mean of the directional hydraulic conductivities.

Note that the flow boundary conditions are the same for both versions of the Henry problem and consist of: no flow boundary conditions at the top and bottom of the confined aquifer; a constant flux along the inland boundary; and a hydrostatic pressure distribution along the seaside boundary. In both versions, a concentration equal to 0 is prescribed along the inland boundary. However, in the dispersive version, the concentration along the seaside boundary is imposed only for the entering fluxes.

Extension to 3D

The model setup is a direct extension of the 2D anisotropic dispersive Henry problem (Abarca et al. 2007a). The geometry of the domain is a rectangular prism (Fig. 1). As the mathematical dimensionless formulation was already presented in 2D in Abarca et al. (2007a), only its 3D extension in dimensionless form will be presented here. First, the dimensionless coordinates and the longitudinal and lateral shape ratios ξ_{xoz} and ξ_{xoy}, respectively are defined (Fig. 1):

$$x_D = \frac{x}{d}, y_D = \frac{y}{d}, z_D = \frac{z}{d}, \xi_{xoz} = \frac{L}{d} \text{ and } \xi_{xoy} = \frac{l}{d} \tag{1}$$

where d [L] is the thickness of the aquifer, L [L] is the distance between the coast and the inland boundary and l [L] is the lateral extension parallel to the shoreline. The freshwater inland boundary is located at x_D=0 and the sea is at $x_D = \xi_{xoz}$. Following Abarca et al. (2007a), the dimensionless head h_D, Darcy velocity q_D, and salt concentration C_D are defined as:

$$q_D = \frac{q}{q_b}, h_D = \frac{hK_{xx}}{q_b d}, \text{ and } C_D = \frac{C}{C_s} \tag{2}$$

where q_b [L/T] represents the prescribed Darcy velocity of the freshwater flux at the inland boundary, q [L/T] the Darcy velocity in the domain, h [L] the equivalent freshwater head, K_{xx} [L/T] the xx component of the hydraulic conductivity tensor, C [M/L^3] the salt concentration, and C_s [M/L^3] the salt concentration of the seawater. Note that the hydraulic conductivity tensor $\boldsymbol{K}$ is assumed to be anisotropic but its main axes are aligned with the coordinate axis. Therefore, $\boldsymbol{K}$ is diagonal. The anisotropy ratios are defined as $r_{yx} = \frac{K_{yy}}{K_{xx}}$ and $r_{zx} = \frac{K_{zz}}{K_{xx}}$. With those definitions, the steady state flow equation in a 3D homogenous medium is expressed as:

$$\frac{\partial^2 h_D}{\partial {x_D}^2} + r_{yx}\frac{\partial^2 h_D}{\partial {y_D}^2} + r_{zx}\frac{\partial^2 h_D}{\partial {z_D}^2} + \frac{1}{a}\frac{\partial C_D}{\partial z_D} = \frac{\varepsilon}{1+\varepsilon C_D} q_D \cdot \nabla' C_D \tag{3}$$

where $a = \frac{q_b}{\varepsilon K_{zz}}$, $\varepsilon = (\rho_s - \rho_0)/\rho_0$ with ρ_s being the fluid density of the seawater and ρ_0 the freshwater density, and ∇' is the gradient written in dimensionless coordinates. As

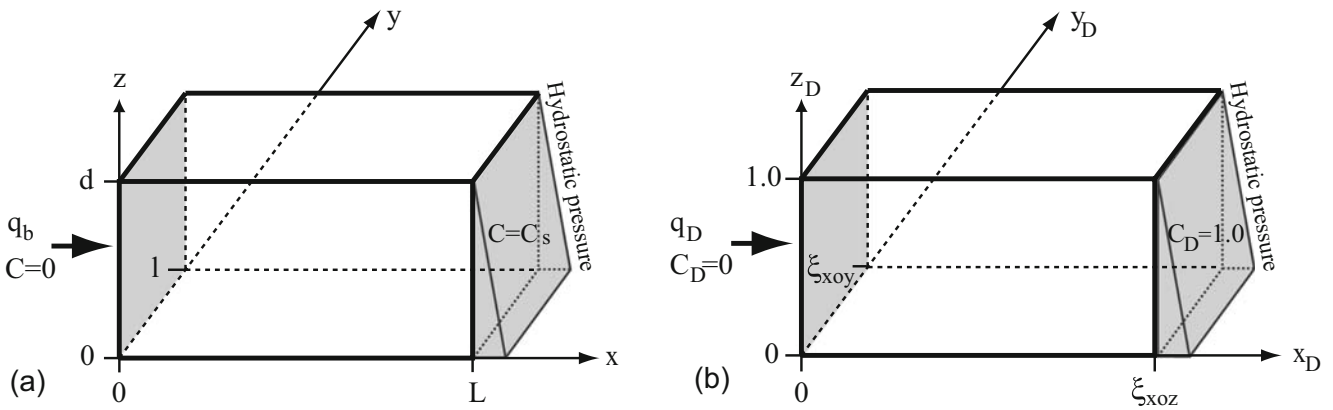

Fig. 1 Model geometry and boundary conditions: **a** real dimensions, **b** dimensionless. Boundary conditions for flow are: no flow conditions on top, bottom and lateral faces of the block, a prescribed flux (q_b) along the inland boundary and a constant hydrostatic head on the seaside boundary. Boundary conditions for transport are: $C = 0$ prescribed along inland boundary fluxes and $C = C_s$ for the inflowing seawater along the seaside boundary

 DOI 10.1007/s10040-009-0533-0

for the standard Henry problem, the boundary conditions are no-flow conditions on the top, bottom and lateral faces of the block, and a prescribed flux (q_b) along the inland boundary:

$$\left.\frac{\partial h_D}{\partial y_D}\right|_{y_D=0,1}=0,\left.\frac{\partial h_D}{\partial z_D}\right|_{z_D=0,1}=0,\left.\frac{\partial h_D}{\partial x_D}\right|_{x_D=0}=-1 \tag{4}$$

A hydrostatic pressure distribution is prescribed along the seaside boundary:

$$h_D(x_D=\xi_{xoz},y_D,z_D)=\frac{1}{r_{zx}\,a}\left(\frac{1}{\varepsilon}+1-z_D\right) \tag{5}$$

The advective-dispersive salt transport equation is then written as:

$$q_D\cdot\nabla' C_D-\nabla'\cdot[b_L\mathbf{D_D}+b_m I]\nabla' C_D=0 \tag{6}$$

with $\mathbf{D_D}$ the dimensionless dispersion tensor, $\mathbf{I}$ is the identity matrix, b_m is the inverse of the Peclet number corresponding to the molecular diffusion (D_m) and b_L is the dimensionless longitudinal dispersivity:

$$b_m=\frac{D_m\phi}{q_b d},\ b_L=\frac{\alpha_L}{d}. \tag{7}$$

with ϕ is the porosity. The ratio of transverse to longitudinal dispersivities is defined by

$$r_\alpha=\frac{\alpha_T}{\alpha_L}, \tag{8}$$

and the components of the dimensionless dispersivity tensor are:

$$D_D^{ij}=r_\alpha\|q_D\|\delta^{ij}+(1-r_\alpha)\frac{q_D{}^i q_D{}^j}{\|q_D\|}. \tag{9}$$

where δ^{ij} denotes the Kronecker delta. The transport boundary conditions are the classical ones (Fig. 1). A dimensionless concentration of 0 is prescribed along the inland side of the domain (x_D=0), a zero mass flux is prescribed on the top, bottom and lateral boundaries, while the boundary condition along the seaside is:

$$q_D C_D|_{x_D=0}-[b_L D_D+b_m I]\nabla' C_D|_{x_D=0}. \tag{10}$$

$$\phi=\begin{cases} q_D C_D|_{x_D=0} & if \quad q_D>0 \\ q_D & if \quad q_D<0 \end{cases}$$

In comparison with the 2D problem (Abarca et al. 2007a), it was necessary to accommodate one additional spatial coordinate (y_D). This leads to the addition of a new hydraulic conductivity anisotropy ratio $r_{yx}=\frac{K_{yy}}{K_{xx}}$. All the rest remains unchanged. Therefore, the dynamic of this problem is controlled by six dimensionless parameters:

$$a,\ b_m,\ b_L,\ r_\alpha,\ r_{yx}=\frac{K_{yy}}{K_{xx}},\ and\ r_{zx}=\frac{K_{zz}}{K_{xx}}. \tag{11}$$

The parameter values used in the numerical model are shown in Table 2.

Extension to the heterogeneous case

The deterministic mathematical model described in the previous section can be applied to solve numerically SWI in heterogeneous media or to perform stochastic modelling. In this work, and for the sake of simplicity it is assumed that the local value of hydraulic conductivity $K(x,y,z)$ is heterogeneous but isotropic. In this case, Darcy's law can be expressed in dimensionless form as follows:

$$q_D^x=-K_D\frac{\partial h_D}{\partial x_D},q_D^y=-K_D\frac{\partial h_D}{\partial y_D}\ and\ q_D^z=-K_D\frac{\partial h_D}{\partial z_D}-K_D\frac{C_D}{a} \tag{12}$$

with the dimensionless hydraulic conductivity K_D defined as $K_D=\frac{K(x,y,z)}{K_g}$, where K_g is the geometric mean of the local hydraulic conductivity values.

The spatial heterogeneity of the hydraulic conductivity is modelled using a multi-Gaussian random function model. A Gaussian distribution and a spherical variogram model of the natural logarithm of the hydraulic conductivities $Y=ln(K)$ were assumed for both 2D and 3D configurations. Note that μ_Y and σ_Y are the mean and the standard deviation of Y respectively. Very often, the ranges of the variogram in the horizontal directions (horizontal correlation lengths λ_x and λ_y) are one order of magnitude larger than in the vertical direction (Gelhar 1986). For the case of identical correlation lengths in the three directions ($\lambda_x=\lambda_y=\lambda_z$), the medium is considered statistically isotropic while it is considered statistically anisotropic if not. The dimensionless directional correlation lengths are: $l_x=\lambda_x/d$, $l_y=\lambda_y/d$ and $l_z=\lambda_z/d$. The level of the heterogeneity of the medium depends on the variance (σ_Y^2) of the random variable.

Stochastic model and analysis

The 2D configurations previously studied by Dagan and Zeitoun (1998), Held et al. (2005), Abarca (2006) or Al-Bitar and Ababou (2005) can be considered as some particular cases of 3D fields if one considers infinite correlation lengths in the horizontal directions as in Dagan and Zeitoun (1998), infinite correlation length along the coastline as in Abarca (2006) and Held et al. (2005), or infinite correlation length in the vertical direction as in Al-Bitar and Ababou (2005). Here, the transition from a 2D vertical cross-section to a full 3D case is investigated. Starting from a 3D heterogeneous medium having an

 DOI 10.1007/s10040-009-0533-0

infinite correlation length parallel to the coast and therefore displaying only a 2D flow system (identical on all the vertical sections), one can progressively reduce the correlation length parallel to the coast to investigate the transition from a 2D situation to a fully 3D one.

Hydraulic conductivity fields

The following is a description of the method used to generate the various sets of hydraulic conductivity fields that are later used to investigate systematically the transition from 2D to 3D and from homogeneous to highly heterogeneous media and its influence on the behaviour of the SWI. Note that the parameters were chosen in a way that the transition could be studied but also in a way that the numerical resolution of the equations is sufficiently accurate. Furthermore, to obtain a statistical representivity of the results the correlation length along the flow direction was kept sufficiently small.

2D and 3D heterogeneity

The shape ratios for the 2D and 3D models are $\xi_{xoz}=2$ and $\xi_{xoy}=1$. All the hydraulic conductivity fields were generated using the Turning Band method (Matheron 1973; Tompson et al. 1989) because it reproduces accurately the target variogram. Two sets of hydraulic conductivity fields were generated. The *isotropic* set corresponds to seven 3D fields that are isotropic in the *xoz* plane and 100 2D isotropic fields. They were generated starting from a 3D hydraulic conductivity field having correlation lengths $l_x = l_y = l_z = 0.04$, a geometric mean $K_g=0.01$ [m/s] and a standard deviation $\sigma_Y=1$. Then, the correlation length in the y direction (l_y) was progressively increased in six steps, until it largely exceeded the size of the domain. All other parameters (l_z, K_g and σ_Y) were kept constant. Figure 2 shows a sample of the *isotropic* 3D fields. The 100 2D fields were generated with the same statistics. Note that these fields share the same statistical parameters ($l_x = l_z = 0.04$, $K_g=0.01$ [m/s] and $\sigma_Y=1$) as the 2D isotropic fields used by Abarca (2006) and Held et al. (2005). The *anisotropic* set corresponds to seven 3D and 100 2D anisotropic fields. A first 3D anisotropic field ($l_x=0.12$, $l_y=0.04$, and $l_z=0.04$) was generated. Its geometric mean and standard deviation are identical to the isotropic case ($K_g=0.01$ [m/s], $\sigma_Y=1$). l_y was then increased in six steps as for the isotropic set. 100 2D anisotropic fields (sharing the same statistics, $l_x=0.12$, $l_z=0.04$) were also generated (Table 1).

To ensure an accurate resolution of the flow and transport equations even for the heterogeneous cases, the 3D models were discretized into 256×128×128 grid cells (more than 4.27 million nodes) while the 2D models were discretized into 256×128 grid cells. The shortest correlation length for the isotropic case corresponds to 5.12 times the grid cell size (avoiding a too large contrast of hydraulic conductivity between two adjacent cells) and to 2% of the size of the domain in the x direction and 4% of the size of the domain in the y and z directions (allowing a statistical representativity of the internal fluctuations within a given model).

Table 1 Dimensions and statistics of the hydraulic conductivity fields

Parameter	Value
Domain size ξ_{xoz} and ξ_{xoy} [–]	2 and 1
Domain discretization Δx_D, Δy_D and Δz_D [–]	0.0078125
$ln(k_D$ [–]) distribution	Gaussian
Variogram type	Spherical
Geometric mean (k_D [–])	0.01
$ln(k_D$ [–]) variances	0.5, 1, 2, 3[a]
Ranges along x (l_x) [–]	0.04, 0.12
Ranges along y (l_y) [–]	0.04, 0.06, 0.1, 0.2, 0.5, 1, +∞
Range along z (l_z) [–]	0.04
Total number of 2D simulations	700
Total number of 3D simulations	49

[a] Only for the isotropic set

Increasing the level of heterogeneity

To investigate the effect of increasing levels of heterogeneity, the $ln(K)$ simulations described above (2D and 3D models) were transformed as follows:

$$Y(\mu_Y, \sigma_Y) = (Y_0 - \mu_Y).\frac{\sigma_Y}{\sigma_{Y0}} + \mu_Y \quad (13)$$

where Y_0 represent the random variable corresponding to an initial simulated field having a mean equal to μ_Y and a standard deviation equal to σ_{Y0}. $Y(\mu_Y,\sigma_Y)$ is the transformed random variable having the same mean μ_Y as the initial one but having a different variance σ_Y. For the isotropic case, four levels of σ_Y^2 : 0.5, 1, 2 and 3 were studied while only three level of σ_Y^2 : 0.5, 1, and 2 were studied for the anisotropic case. This led to four sets of 100 2D simulations which will be compared depending on the $ln(K)$ variance to four sets of seven 3D simulations in the isotropic case; and three sets of 100 2D simulations which will be compared to three sets of seven 3D simulations in the anisotropic case. Note that in all cases, the geometric mean of the hydraulic conductivity is equal to $K_g=0.01$ [m/s].

Effective hydraulic parameters

Effective hydraulic conductivity

For each configuration, the effective directional hydraulic conductivity tensor of the heterogeneous fields was estimated with Ababou (1996) formula:

$$K_{ef,ii} = K_g \exp\left(\sigma_Y^2\left[\frac{1}{2} - \frac{1}{N}\frac{\lambda_h}{\lambda_i}\right]\right) \quad (14)$$

where K_g is the geometric mean of the hydraulic conductivity [m/s]; σ_Y^2 is the $ln(K)$ variance; N is the number of dimensions; λ_i is the correlation length [m] in the direction i and λ_h is the harmonic mean of the

 DOI 10.1007/s10040-009-0533-0

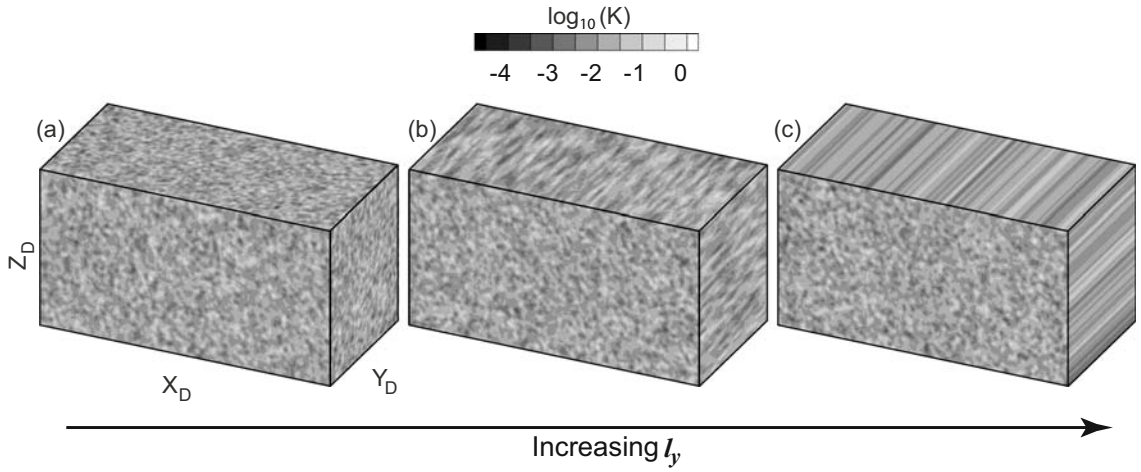

Fig. 2 View of the 3D hydraulic conductivity fields. For all cases $l_x = l_z$=0.04, K_g=0.01 [m/s] and σ_Y=1 are constant: **a** l_y=0.04 (statistically isotropic case); **b** l_y=0.5; **c** $l_y = +\infty$. Note that **c** is equivalent to Abarca (2006) and Held et al. (2005) cases

correlation lengths [m]. This formula is a generalization of Matheron's conjecture (Matheron 1967) applicable for the 3D anisotropic multi-Gaussian media. It is worth noting that this formula does not account for density variations. The resulting effective hydraulic conductivities are shown in Fig. 3. The maximum anisotropy ratios are r_{yx}=4.48 (obtained for $l_x = l_z$=0.04, $l_y = +\infty$, $\sigma_Y^2 = 3$) and r_{zx}=0.36 (l_x=3 × l_z=0.12, $l_y = +\infty$, $\sigma_Y^2 = 2$). For comparison and validation reasons, equivalent hydraulic conductivities were also calculated numerically by solving steady state flow with constant hydraulic gradients and provided similar results.

It is important to note that in a 2D multi-Gaussian isotropic medium, the effective horizontal and vertical hydraulic conductivities are equal to the geometric mean and independent of *ln*(*K*) variance. As shown in Fig. 3, when the variance increases in statistically anisotropic media the effective hydraulic conductivity in the direction

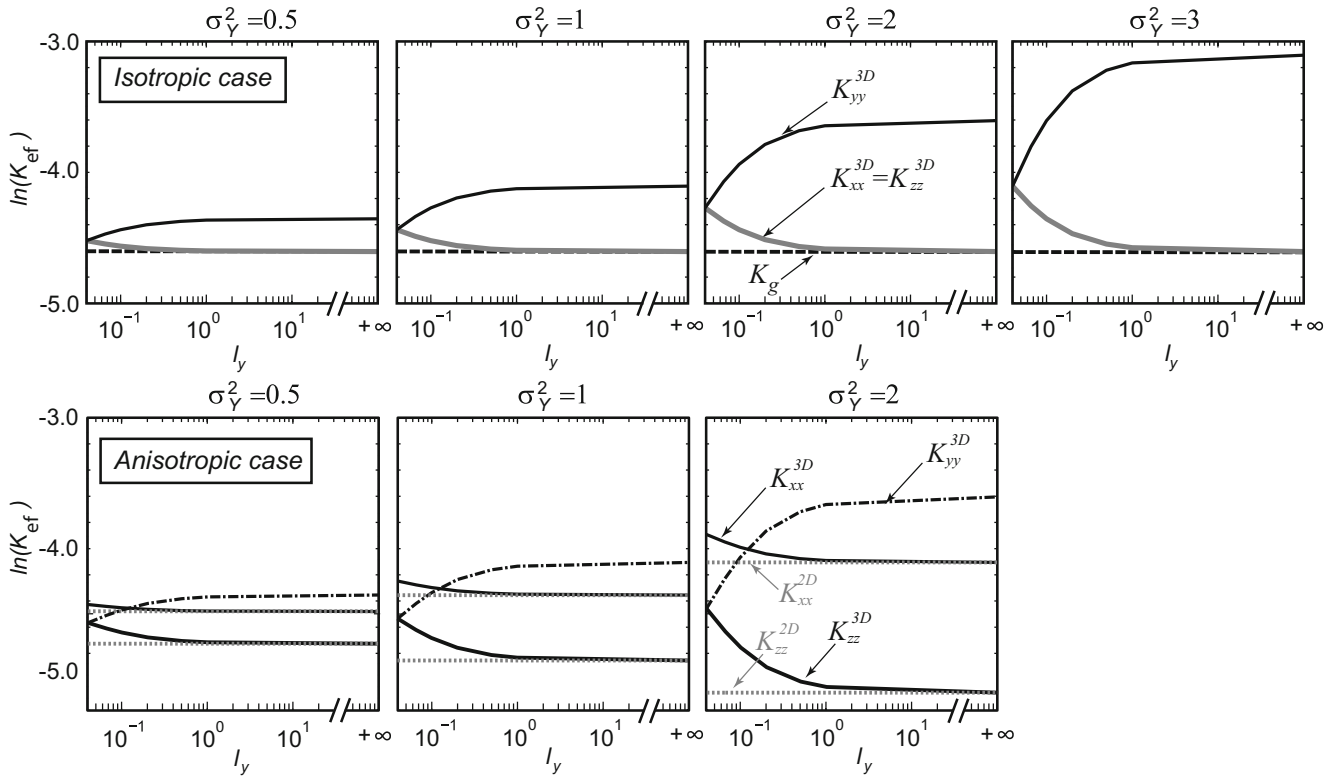

Fig. 3 Evolution of the effective directional hydraulic conductivities K_{ef} as a function of increasing l_y for different levels of *ln(K)* variances in the 3D and 2D models. In upper row graphs concerning the isotropic case, line types correspond to the same variables as indicated in the third one. In lower row graphs concerning the anisotropic case, line types correspond to the same variables as indicated in the third one

 DOI 10.1007/s10040-009-0533-0

parallel to the stratification (longest correlation length) tends toward the arithmetic mean, while it tends to the harmonic mean in the perpendicular direction.

Effective dispersivities

An important question was whether effective dispersivities should be used or not; and if they needed to be use, how to estimate them in a simple manner? It was decided to use the same values for the longitudinal and transversal dispersivities for both the heterogeneous and homogenous media (2D and 3D). This allowed for testing as to whether the use of the local dispersivities is sufficient to provide acceptable homogenized results. The use of scale invariant dispersivities was motivated by the absence of an appropriate analytical model at the scale and level of heterogeneity that are investigated in the numerical simulations. Indeed, the results obtained by spectral perturbation techniques to calculate effective dispersivities as in Welty and Gelhar (1991), Welty et al. (2003) and Dentz et al. (2000) are valid for weakly heterogeneous media. In addition, the dispersive Henry problem is characterized by high local dispersivity coefficients as compared to the correlation length of the heterogeneity (α_L=0.1 and l_x=0.04 or 0.12), while the expressions of effective dispersivity usually assume $\alpha_L << l_x$, e.g. Welty and Gelhar (1991) and Welty et al. (2003). Finally, Held et al. (2005) used the homogenization theory to derive expressions for the heterogeneous Henry problem. They found that the effective longitudinal and transversal dispersivities correspond closely to the local values. However, in their numerical analysis, Held et al. (2005) considered high molecular diffusion (even in their dispersive case), and low $ln(K)$ field variance (equal to 1).

Density-dependent flow and solute transport Monte Carlo simulations

The coupled variable-density flow and advective-dispersive solute transport equations were solved with the finite element code *GroundWater* (Cornaton 2007) for both the 2D and 3D configurations. The code has been previously validated by comparison with a series of standard published benchmarks including comparison with pseudo-analytical solutions such as the Henry problem or numerical experiments such as the Elder or the Hydrocoin Case 5 Level 1 problems. The Boussinesq approximation and constant fluid viscosity were used because of the small density contrast between fresh and saltwater. The model geometry and boundary conditions (Fig. 1) are described in section Extension to 3D. The 3D models are discretized into 256×128×128 elements while the 2D models are discretized into 256×128 elements (the same as for the hydraulic conductivity fields). Finer numerical resolutions were tested to check the accuracy of the solution but these tests did not show any significant effect of refining the numerical mesh. Therefore the previous resolution was kept among the simulations. For each numerical simulation a different hydraulic conductivity field is used. The other parameters are kept constant (Table 2). Following standard methodology, the transport is computed by solving a transient transport problem until the concentration reaches an equilibrium value. A series of preliminary simulations showed that the steady state transport regime was reached in less than 0.75 day which was then used as the fixed duration for all the 2D and 3D simulations.

Table 2 Used model parameters

Symbol	Parameter	Value	Units
K_g	Geometric mean conductivity	$1.00\ 10^{-2}$	m/s
ϕ	Porosity	0.35	–
D_m	Molecular diffusion coefficient	0.00	m^2/s
α_L	Horizontal longitudinal dispersion	0.10	m
α_L[a]	Horizontal transversal dispersion	0.10	m
α_T	Vertical transversal dispersion	0.01	m
q_b	Inland freshwater flux	$6.60\ 10^{-5}$	m/s
ρ_0	Freshwater density	$1.00\ 10^{3}$	kg/m^3
ρ_S	Seawater density	$1.025\ 10^{3}$	kg/m^3
μ	Fluid viscosity	$1.00\ 10^{-3}$	kg/m/s

[a] Only in three-dimensional models

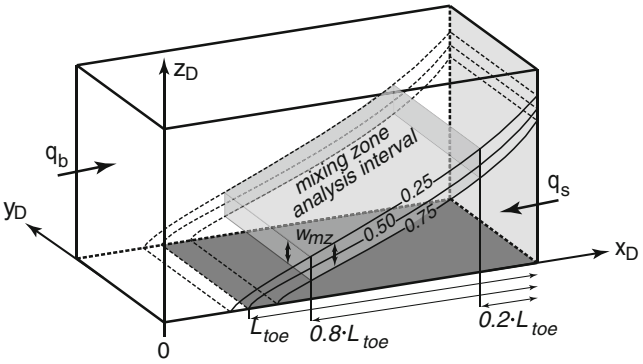

Fig. 4 Evaluation criteria. L_{toe} represents the toe penetration length, q_s the seawater inflowing flux and w_{mz} the width of the mixing zone

The results of the flow simulations are characterized by three parameters borrowed from Abarca et al. (2007a). Two parameters describe the geometry of the freshwater/seawater interface (length and width), and the third measures the amount of saltwater entering the system (Fig. 4). In order to avoid scale-dependent analysis, all parameters are dimensionless and defined as follows:

- Dimensionless penetration length of the saltwater wedge $L_D = L_{toe}/d$: the distance L_{toe} between the seaside boundary and the point where the relative isoconcentration C_D=0.5 intersects the bottom of the aquifer normalized by the aquifer thickness d.
- Dimensionless width of the mixing zone $W_D = w_{mz}/d$: the average vertical width w_{mz} of the area between the relative isoconcentrations C_D=0.25 and C_D=0.75 and between 0.2 L_{toe} and 0.8 L_{toe} normalized by the aquifer thickness d.
- Dimensionless saltwater inflowing flux $R_D = q_s/q_b$: the saltwater inflowing flux q_s normalized by the inflowing freshwater flux q_b.

DOI 10.1007/s10040-009-0533-0

For the heterogeneous 2D cases, ensemble averages of the criteria over 100 simulations were calculated as follows:

$$L_D^{2DHet.} = \frac{1}{n}\sum_{sim=1}^{n} L_D^{sim}, \qquad (15)$$

$$W_D^{2DHet.} = \frac{1}{n}\sum_{sim=1}^{n} W_D^{sim} \text{ and } R_D^{2DHet.} = \frac{1}{n}\sum_{sim=1}^{n} R_D^{sim}$$

where n is the number of 2D simulations, and "sim" refers to one 2D simulation.

In 3D, the CPU time required to run the complete set of 3D simulations needed for all the configurations investigated in this study would have required about 500 days (on a Linux AMD Opteron 64 bits machine) to run 100 simulations per configuration. To reduce the computing time, spatial averages on single 3D simulations were used instead of ensemble averages on many simulations. In other words, it is assumed that for one 3D realization, the spatial averaging of flow and transport solutions along the y direction (parallel to the shoreline) will give the same ensemble statistics (average and variance) than multiple 3D realizations (ergodicity assumption):

$$L_D^{3DHet.} = \frac{1}{ns}\sum_{slice=1}^{ns} L_D^{slice}, \qquad (16)$$

$$W_D^{3DHet.} = \frac{1}{ns}\sum_{slice=1}^{ns} W_D^{slice} \text{ and } R_D^{3DHet.} = R_D^{sim}$$

where ns is the number of 2D vertical slices in a 3D model, and slice refers to one "slice" of a 3D model (128 slices). A similar assumption was used by Al-Bitar and Ababou (2005). In the following, the ergodicity assumption is tested numerically for three configurations.

Numerical results

Ergodicity hypothesis

The ensemble statistics of the 3D salt concentration distribution along the central slice of the model (y_D=0.5) calculated over 100 3D realizations are compared with the spatial statistics calculated on a single realization with Eq. (16). The 3D hydraulic conductivity fields have the following correlation lengths l_x=0.12, l_y=0.12, l_z=0.04. The numerical test has been conducted for three levels of $ln(K)$ variance: 1, 2 and 3. It was found that the ensemble average concentrations (grey lines on Figs. 5a,c,e) are well approximated by the spatial mean (grey lines on Figs. 5b, d,f). Similarly, the ensemble concentration variance (background greymaps in Figs. 5a,c,e) are well approximated by the spatial concentration variance (Figs. 5b,d,f) even for a large $ln(K)$ variance $\left(\sigma_Y^2 = 3\right)$. Figure 5 shows also that the ensemble estimates are smoother and more regular than the spatial estimates. In terms of estimation of the mean position of the toe, the test shows that the spatial average performs very well (Table 3); the width of the mixing zone is estimated reasonably well, but the variances are much less accurate both for the position of the toe and the width of the mixing zone (Table 3). Therefore, the ergodicity assumption can be accepted, but results concerning the estimated variances must be interpreted with care. In addition, for large correlation lengths in the y direction, the ergodicity assumption is certainly not reasonable any more.

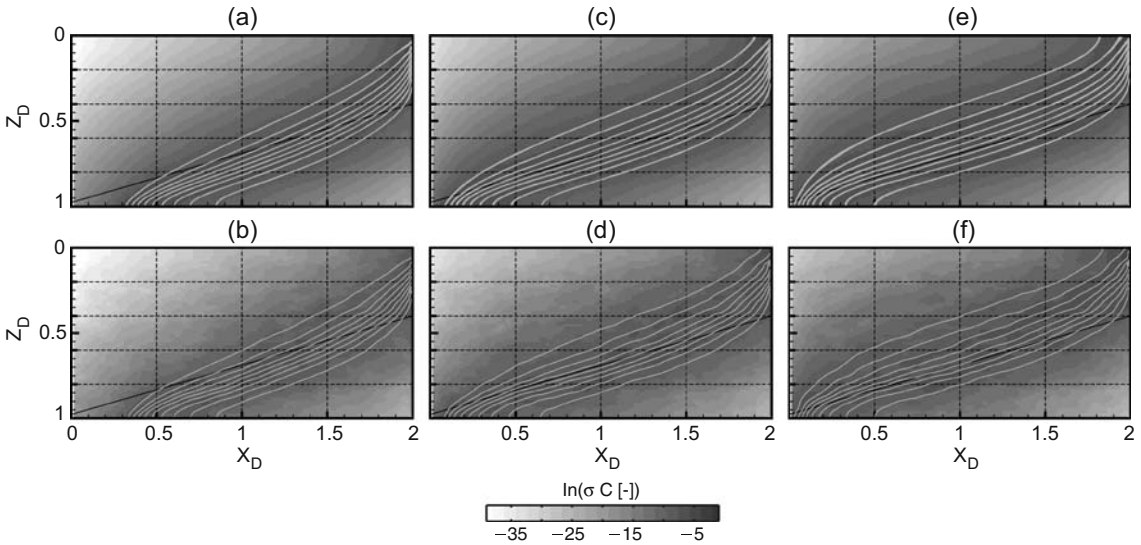

Fig. 5 Ergodicity test: upper row (**a**, **c**, **e**): 2D vertical cross-section (y_D=0.5) of the ensemble average relative salt concentration [–] isolines (0.1–0.9) and the ensemble variance (*background greyscale map*) calculated on 100 3D simulations. Lower row (**b**, **d**, **f**): 2D view of the spatial average relative salt concentration [–] isolines (0.1–0.9) and the spatial variance calculated on a single 3D simulation. *Greyscale maps* represent the natural logarithm of the variance. The results are presented for $l_x = l_y$=0.12 l_z=0.04 and the three cases of *ln* (*K*) variance $\left(a - b\ \sigma_Y^2 = 1,\ c - d\ \sigma_Y^2 = 2,\ e - f\ \sigma_Y^2 = 3\right)$

 DOI 10.1007/s10040-009-0533-0

Table 3 Comparison between ensemble and spatial statistics (EA refers to ensemble average, SA refers to spatial average)

σ_Y^2	$\frac{L_D^{EA}}{L_D^{SA}}$	$\frac{\sigma_{LD}^{EA}}{\sigma_{LD}^{SA}}$	$\frac{W_D^{EA}}{W_D^{SA}}$	$\frac{\sigma_{WD}^{EA}}{\sigma_{WD}^{SA}}$
1	1.01	1.34	0.96	0.56
2	1.00	1.55	1.02	0.63
3	1.00	0.71	1.02	0.83

Preliminary results

To start the analysis, a single realization in 2D and another one in 3D sharing the same parameters and the same distribution (histogram) of hydraulic conductivity are considered. Figure 6 shows the 2D vertical cross-sections of the relative salt concentration isolines calculated considering the heterogeneous medium (solid line) or considering a homogenous medium (dashed line) whose equivalent hydraulic conductivity was calculated with Eq. (14). Note that for the 2D case, only one realization is shown whereas for the 3D case the lateral average (in the y direction) of salt concentrations is shown. By visual comparison, it is clear that the solid lines and dashed lines do not match indicating that in all the cases there is a difference in the concentration fields between the homogenous and heterogeneous cases. The difference increases as σ_Y^2 increases (compare Fig. 6b and d and compare Fig. 6c and e). Furthermore the magnitude of the difference is larger in 2D than in 3D (compare Fig. 6b and c and compare Fig. 6d and e).

More generally, the comparison of the isoconcentration contours, head and permeability fields allows characterizing the behaviour of the saltwater wedge as follows:

- In 2D and in 3D, the concentration gradients are higher in the low permeable zones than in the high permeable zones.
- The organization of heterogeneity, especially isolated high permeability zones along the sea boundary, might

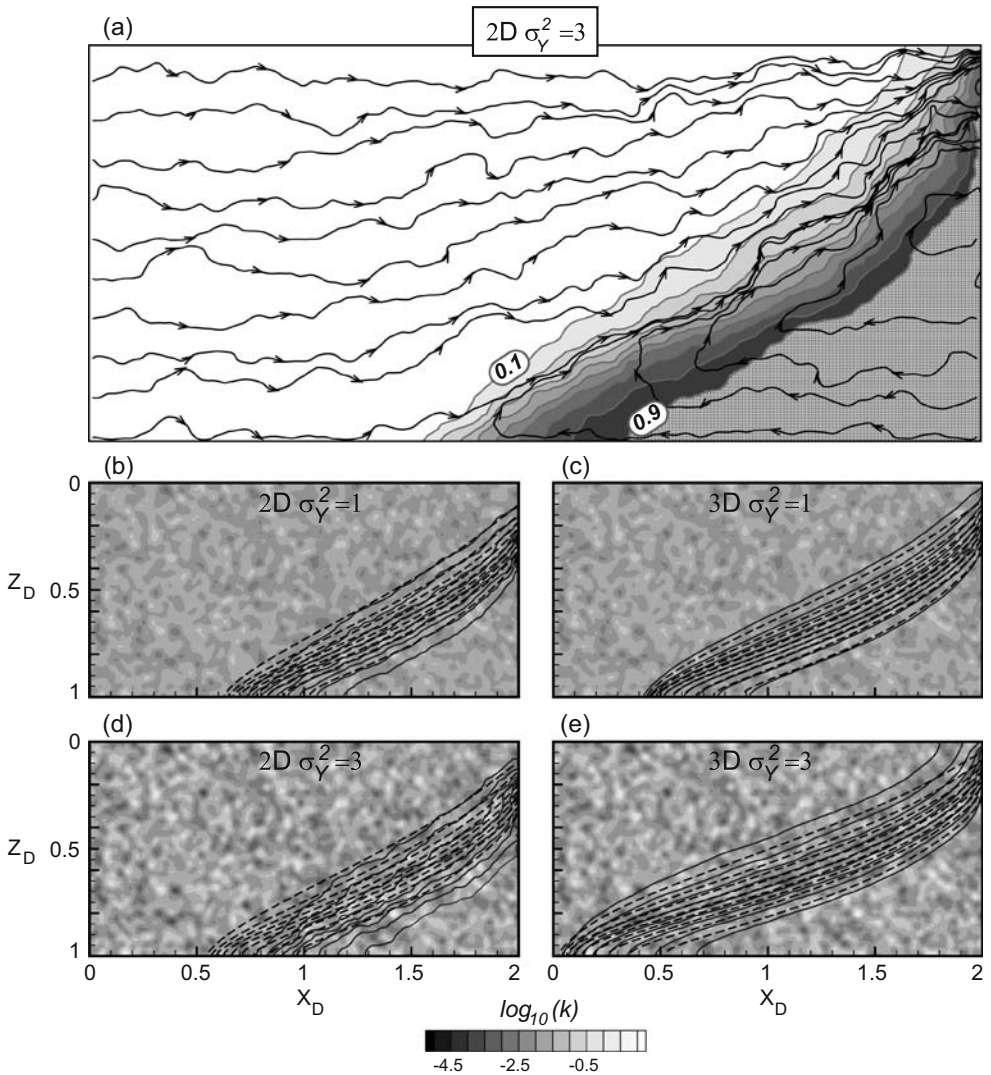

Fig. 6 **a** Streamlines and dimensionless concentration contours for a single 2D isotropic realization of variance of 3 (the size of this figure is exaggerated); 2D vertical cross-section views of concentration [–] isolines (0.1–0.9): **b** for the 2D heterogeneous isotropic case (*solid line*) and homogenous case (*dashed line*); **c** for the 3D heterogeneous isotropic case (*solid line*) and homogenous (*dashed line*). For both cases $\sigma_Y^2 = 1$. Parts **d** and **e** are the same as parts **b** and **c** except for for $\sigma_Y^2 = 3$

 DOI 10.1007/s10040-009-0533-0

lead to the apparition of small scale convection cells depending on the *ln(K)* variance.
– One can observe a rotation (seaward and upward shift of the saltwater wedge) of the freshwater/saltwater interface in 2D heterogeneous models as compared to the 2D homogenous models. The same behaviour is less visible in the 3D configuration.

Those effects of 2D heterogeneity are in agreement with previous findings (Held et al. 2005; Abarca 2006). Yet, these studies investigated the effects of 2D heterogeneity with hydraulic conductivity variance up to 2.

Impact of the heterogeneity

This section focuses on the description of the effect of heterogeneity on SWI. The effects of the heterogeneity are investigated by comparing the dimensionless characteristics L_D, W_D and R_D obtained for heterogeneous media with the corresponding dimensionless parameters obtained for the effective homogenous media. The comparison is carried out separately for 2D and 3D isotropic and anisotropic configurations and for increased levels of $ln(K)$ variance.

The results are presented in Table 4. The first observation is that all the ratios deviate more significantly from 1.00 in the 2D cases than in the 3D cases. This shows that the difference between heterogeneous and their equivalent homogeneous media is higher in 2D than in 3D. One can also note that the difference increases when increasing σ_Y^2. Another observation is that the steady inflowing saltwater flux R_D is the parameter which is the most affected by the hydraulic conductivity heterogeneity since it can be more than 20 times larger in heterogeneous models than in the homogenous models with identical effective directional hydraulic conductivity ($\sigma_Y^2 = 3$). The magnitude of R_D is always much larger in the heterogeneous cases than in the homogenous ones, and it increases almost exponentially when increasing σ_Y^2. According to Abarca et al (2007a) and in 2D, R_D is controlled by the geometric mean of the hydraulic conductivity and the transversal dispersion.

The differences between the values of R_D computed for the heterogeneous cases and their respective homogenized versions is interpreted as a result of using the local dispersivity instead of an effective dispersivity in the homogenized model. Indeed, the transversal dispersion in the heterogeneous medium is higher than in the homogeneous one due to vertical velocity variations at a small scale. Increasing the transverse dispersivity implies a decrease of the magnitude of the density contrast because of an enhanced mixing between saltwater and freshwater. The increase of transversal dispersivity leads to an increase of R_D to compensate for the loss of brackish water that is captured by the freshwater outflux.

This difference between the heterogeneous and homogenous models might also be explained by the absence of local convection cells in the homogeneous case. These local convection cells appear when high permeability and isolated zones are located along the sea boundary; these situations are more frequent when increasing σ_Y^2. The role of the convection cells is stronger in 2D because the high permeable zones are more isolated in 2D than in 3D.

With regard to L_D and W_D, in all the cases, the saltwater wedge moves seaward when considering heterogeneous models instead of homogenous ones while the width of the mixing zone tends to increase. These two effects can be interpreted in the following manner. One impact of the heterogeneity is to enhance both the longitudinal and transverse (macro) dispersion. When the transverse macro dispersivity normal to the concentration gradients increases, it implies some additional spreading and therefore a larger mixing zone. A consequence of the spreading is a reduction of the density contrast within the mixing zone leading to a rotation of the saltwater wedge: its base moves seaward and its vertical extension increases as shown in Fig. 6. The magnitude of that effect increases with σ_Y^2. Furthermore, the effect is more pronounced in 2D than in 3D because there are more possibilities for flow to go through the low permeability heterogeneities in 3D than in 2D; the flow lines are less distorted and the heterogeneities have less impact on saltwater spreading in 3D than in 2D.

When comparing the effects of isotropic and anisotropic heterogeneity in 2D and 3D configurations, one can see that the trends are similar but slightly more pronounced for the anisotropic media (compare isotropic versus anisotropic values in Table 4). It is interpreted as a consequence of increased velocity in the horizontal direction in the anisotropic case resulting in increased longitudinal and transversal dispersion.

The calculation of the relative salt concentration variance over 100 2D and 100 3D Monte Carlo

Table 4 Comparison between heterogeneous (characteristic norms with *Het.* subscript) versus homogenous (norms with *Hom.* subscript) media

σ_Y^2	0.5	1	2	3	0.5	1	2
	2D isotropic				**2D anisotropic**		
$L_D^{Het.}/L_D^{Hom.}[-]$	0.97	0.95	0.92	0.89	0.94	0.89	0.82
$W_D^{Het.}/W_D^{Hom.}[-]$	1.12	1.24	1.42	1.53	1.15	1.25	1.31
$R_D^{Het.}/R_D^{Hom.}[-]$	3.35	5.98	14.03	28.08	3.46	6.15	14.14
	3D isotropic				**3D anisotropic**		
$L_D^{Het.}/L_D^{Hom.}[-]$	1.02	1.01	0.99	0.97	0.99	0.97	0.95
$W_D^{Het.}/W_D^{Hom.}[-]$	1.04	1.07	1.18	1.21	1.05	1.11	1.17
$R_D^{Het.}/R_D^{Hom.}[-]$	2.38	3.84	7.72	13.35	2.65	4.43	9.22

 DOI 10.1007/s10040-009-0533-0

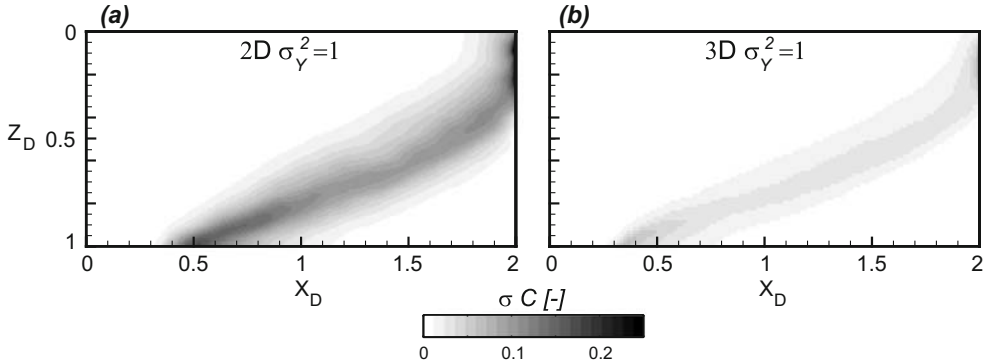

Fig. 7 Ensemble standard deviation of the relative concentrations calculated over: **a** 100 2D simulations with l_x=0.12 and l_z=0.04; **b** 100 3D simulations with $l_x = l_y$=0.12 and l_z=0.04. For both cases $\sigma_Y^2 = 1$

simulations shows (Fig. 7) that the two extremities of the saltwater wedge (near the bottom and freshwater outlet zones) are the most affected by the heterogeneity. The uncertainty increases with increasing σ_Y^2. The uncertainty on the toe and on the freshwater output zone is high because these two structures (stagnation point at the toe, and flow concentration in a narrow area at the outflow face) have a small dimension as compared to the size of the heterogeneities and therefore are very sensitive to variations of the local hydraulic conductivities from one simulation to the other.

Dimensionality effects

As a first illustration of the dimensionality effects, Fig. 8 shows how the seawater intrusion moves farther inland when a full 3D heterogeneity (Fig. 8a) is considered as compared to a 2D heterogeneous model (equivalent to Fig. 8c). Figure 8 shows also that the mixing zone is rougher in 2D than in 3D models.

A more detailed analysis of these effects is displayed in Fig. 9, which shows the mean of the dimensionless norms L_D, W_D, and R_D obtained for 3D models normalized by the results obtained in 2D and plotted as a function of increasing l_y. In other words, Figure 9 illustrates the behaviour of the SWI through the transition from a fully 3D model to a 2D model for different levels of heterogeneity (the different lines). One can see on that figure that the position of the toe L_D is the parameter that is the most affected by model dimensionality. The saltwater wedge penetrates farther landward in 3D than in 2D for both the isotropic and anisotropic cases. Even for small values of σ_Y^2, the landward shift is around 10%. This effect increases when increasing σ_Y^2, and the relative difference between 2D and 3D reaches 38% for $\sigma_Y^2 = 3$.

This is not surprising, because the saltwater wedge penetration is highly dependent on the horizontal hydraulic conductivity (Abarca et al. 2007a), and increasing the dimension of the problem increases the effective hydraulic conductivity in the main flow direction (x direction). The differences between the 2D and 3D situations can be explained on the base of Eq. (14). In 2D, the effective hydraulic conductivity of a statistically isotropic log multi-Gaussian heterogeneous media is the geometric mean; it does not depend on the level of heterogeneity quantified by the variance σ_Y^2. However, for a 3D field, sharing the same statistics as the previous 2D media, the effective hydraulic conductivity is $exp(\sigma_Y^2/6)$ times larger than in 2D. The consequence is that the global pressure gradient between the freshwater flux landside and the seawater hydrostatic pressure is smaller in 3D than in 2D, inducing thus, a landward movement of the saltwater

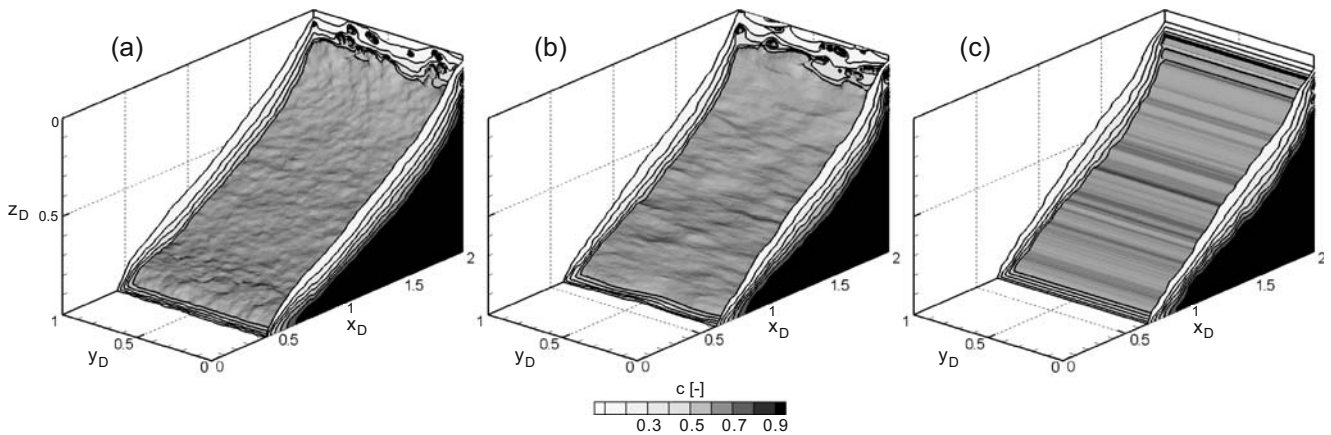

Fig. 8 3D view of the relative salt concentration [–] isolines (0.1–0.9); **a** for the isotropic case with $l_x = l_y = l_z$=0.04, **b** for the case where $l_x = l_z$=0.04 and l_y=0.1, **c** for the case with $l_x = l_z$=0.04 and $l_y = +\infty$. Note that **c** is equivalent to a 2D model. For the 3 cases, the *ln(K)* variance is equal to 1

 DOI 10.1007/s10040-009-0533-0

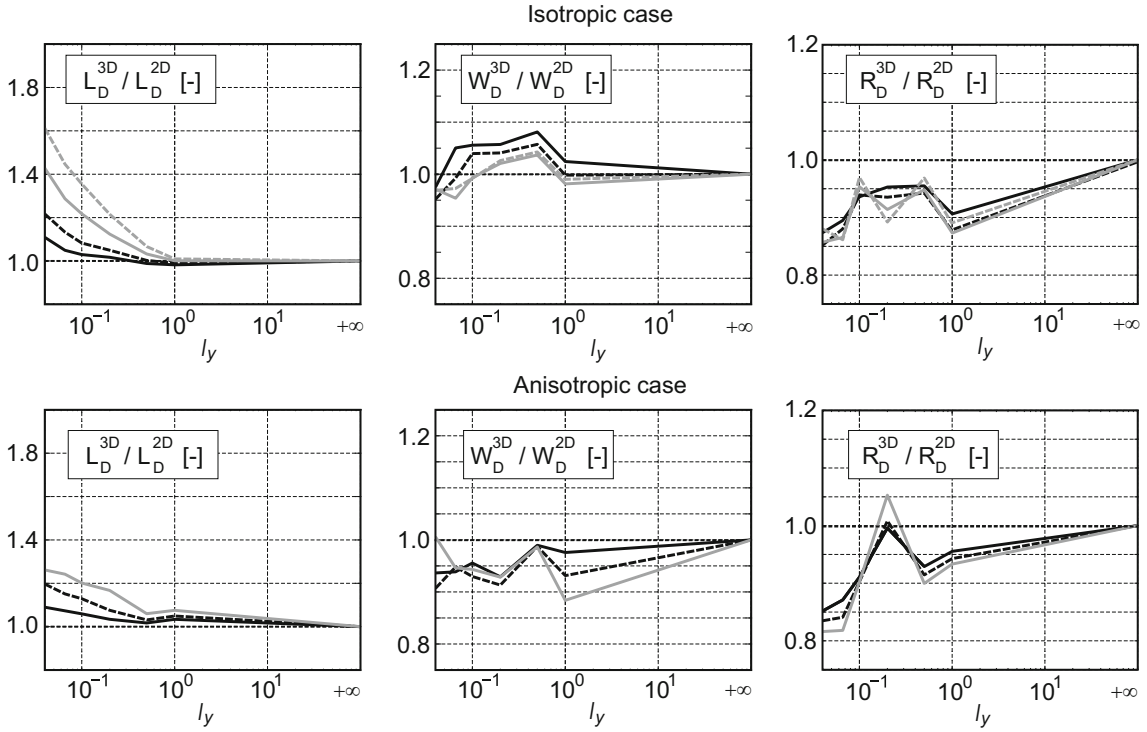

Fig. 9 Dimensionless norms comparison between 2D and 3D for different level of *ln(K)* variance (*solid black line* for $\sigma_Y^2 = 0.5$, *dashed black line* for $\sigma_Y^2 = 1$, *solid grey line* for $\sigma_Y^2 = 2$ and *dashed grey line* for $\sigma_Y^2 = 3$)

interface. This is why the saltwater wedge penetrates further landward in 3D than in 2D configurations.

Furthermore, it has already been shown analytically that the ratio of directional velocity variations ($\sigma_{qV}^2/\sigma_{qH}^2$, where σ_{qV}^2 is the variation of vertical velocity and σ_{qH}^2 is the variation of horizontal velocity) is larger in 2D than in 3D. Indeed, according to Gelhar (1993), for a 2D statistically isotropic medium, the ratio of transverse to longitudinal velocity variation is one third, whereas, it is eight thirds times smaller in 3D. It implies that there is more vertical mixing in 2D, and thus less density effects, which causes the rotation of the saltwater wedge as explained in the previous section. At the same time, even if the geometric mean of longitudinal and transversal dispersivities increases when hydraulic conductivity increases (from 2D to 3D), the dispersion-advection ratio decreases and becomes dominated by the advection transport process leading to a convergence toward a sharp interface (longer penetration and thin mixing zone). Finally, the effective hydraulic conductivity being higher in 3D than in 2D, it implies a reduction of the dimensionless parameter $a = \frac{q_b}{\varepsilon K_{zz}}$ (with respect to Peclet condition) which compares viscosity and buoyancy forces, hence more density effects as discussed by Simpson and Clement (2004).

The width of the mixing zone W_D is also affected by model dimensionality (Fig. 9). The results are not as clear as for the position of the toe probably because of the limits of the ergodicity assumption. Yet, some tendencies can be observed. In all cases, the difference between 2D and 3D does not exceed 10%. In the isotropic case, for small correlation length l_y, W_D in 3D models is smaller than those in 2D, while the reverse for higher correlation lengths. For the statistically anisotropic cases, the width of the mixing zone in 3D models is always smaller than those in 2D even for a higher σ_Y^2. The width of the mixing zone (in homogenous media) depends mostly on the geometric mean of the longitudinal and transversal dispersivities (Abarca et al. 2007a). This suggests that (mechanical) dispersion due to heterogeneity, especially the transversal dispersivity, increases as a function of velocity variance more significantly in 2D than in 3D models. With regard to the inflowing saltwater, the flux in 2D models is larger than in 3D models. This confirms that the dispersion due to the heterogeneity is larger in 2D than in 3D models because R_D is highly controlled by dispersion (Abarca et al. 2007a).

Another difference between the 2D and 3D models is the estimation of the uncertainty of the outputs (variances of L_D, W_D and R_D). Table 5 shows that the 2D models predict a higher uncertainty (up to 5 times) than 3D models. However, the relative variability of $L_D\left(\sigma L_D^{3D}/L_D^{3D}\ or\ \sigma L_D^{2D}/L_D^{2D}\right)$ is slightly larger in 2D but does not exceed 0.03. The same is true for W_D with a maximal value of 0.05. This is attributed to less saltwater spreading in 3D models due to less velocity variability.

Table 5 Comparison between 2D and 3D uncertainty, σ represents the standard deviation

σ_Y^2	Isotropic		Anisotropic	
	$\sigma L_D^{3D}/\sigma L_D^{2D}$	$\sigma W_D^{3D}/\sigma W_D^{2D}$	$\sigma L_D^{3D}/\sigma L_D^{2D}$	$\sigma W_D^{3D}/\sigma W_D^{2D}$
0.5	0.17	0.29	0.20	0.25
1	0.15	0.19	0.29	0.46
2	0.14	0.16	0.22	0.45
3	0.19	0.35	–	–

 DOI 10.1007/s10040-009-0533-0

Effects of increasing variability

Another way to analyse the results, is to study how the saltwater wedge evolves when the degree of heterogeneity (σ_Y^2) increases (Fig. 10). The toe penetration in the 2D models is smaller than in the 3D models, especially when the variance increases.

An interesting behaviour can be observed in the isotropic case: in 2D models, the toe penetration decreases when the variance increases, whereas, in 3D the toe penetration increases significantly when the variance increases for the isotropic media (Fig. 10a). Intermediate behaviour occurs depending on the magnitude of the correlation length in the direction parallel to the coast. In addition, for statistically anisotropic hydraulic conductivity fields, the toe penetration increases when the variance increases in both 2D and 3D settings (Fig. 10c). This complex behaviour is the result, as discussed before, of the combined effect of the effective hydraulic conductivity and macrodispersion. For the isotropic heterogeneous 2D domain, the effective hydraulic conductivity is equal to the geometric mean of $ln(K)$ independently of the value of σ_Y^2. Yet, regardless of dimensionality and isotropic or anisotropic media, increasing the level of heterogeneity increases macrodispersion. In this case, the position of the toe is controlled by the macrodispersion processes which increase with increasing σ_Y^2. It is not the case for the 2D or 3D statistically anisotropic media where the effective hydraulic conductivity increases in the flow direction when σ_Y^2 increases. Figure 10a shows that there is a threshold in the relation between advective and dispersive solute transport for which the toe penetration can increase or decrease, or even remain constant when σ_Y^2 increases.

From 2D to 3D

The previous sections have shown that the behaviour of 3D SWI models is generally different from those of 2D models sharing the same statistical parameters of the hydraulic conductivity fields (except of course the correlation length in the direction perpendicular to the section). This shows that forecasts based only on 2D sections may be inaccurate. In the following, a technique to modify the statistical parameters of the 2D heterogeneous simulations is proposed to approximate the results of a 3D analysis which would be much more CPU demanding. In addition, the modification of the 2D hydraulic conductivity fields will allow the comparison between 2D and 3D field sharing the same effective directional hydraulic conductivities.

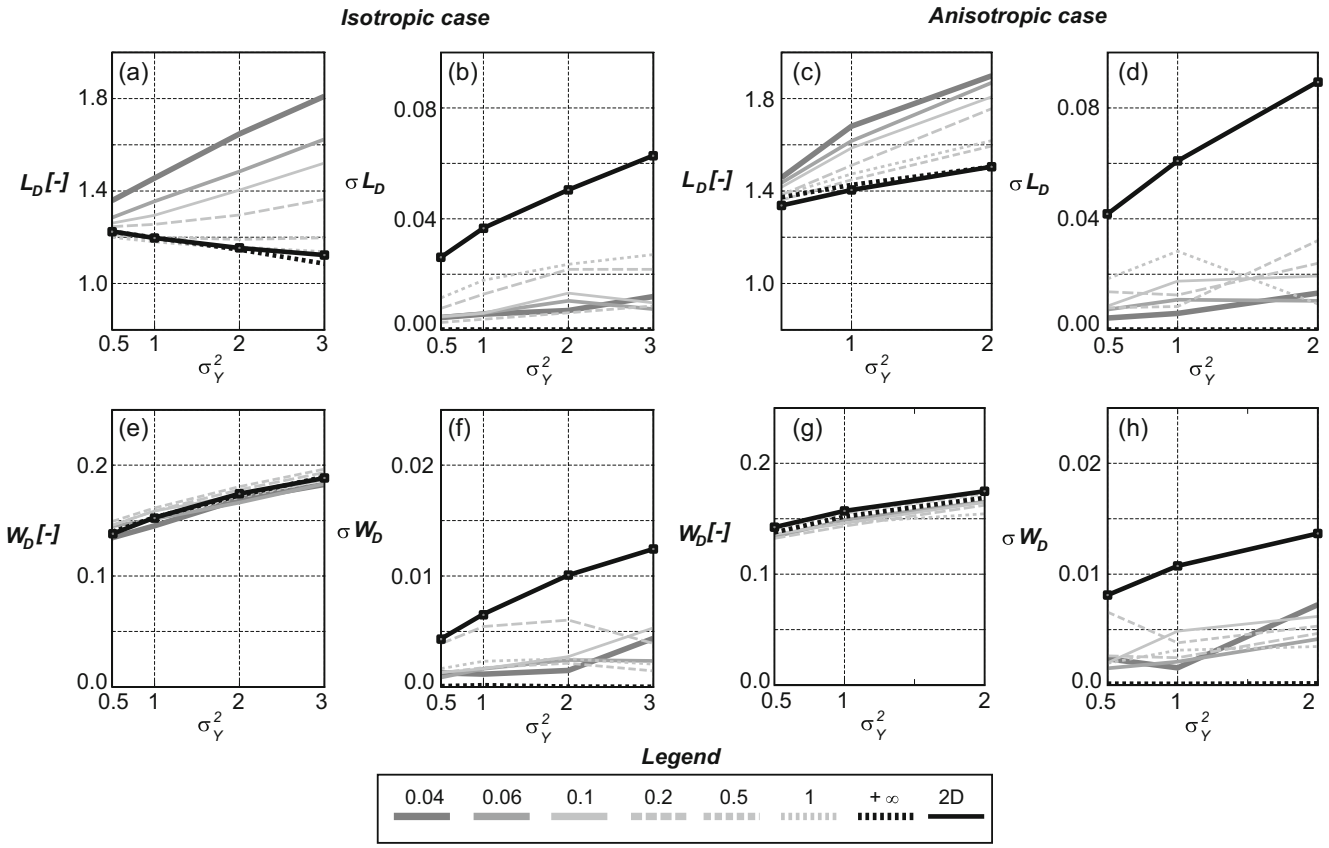

Fig. 10 Evolution of the dimensionless criteria as a function of increasing *ln(K)* variance, (**a**, **b**, **e**, **f**) for the isotropic case and (**c**, **d**, **g**, **h**) for the isotropic case. Note that 2D results (*solid black line*) are compared to 3D model results with increasing l_y from 0.04 (*dark grey line*) to +∞ (*dashed black line*)

 DOI 10.1007/s10040-009-0533-0

2D hydraulic conductivity fields transformation

The basic idea of the proposed methodology is to generate a 2D field having the same correlation lengths and effective hydraulic conductivities in the x and z directions as a 3D field. Assuming a log multi-Gaussian random function and assuming that its parameters in 3D are known, it is possible to express the geometric mean K_g^{2D} and the variance σ^2_{Y2D} of the 2D field from the statistical parameters of the 3D field.

To derive that relation, the first step is to define the correlation lengths of the two fields:

$$\lambda_x^{2D} = \lambda_x^{3D} = \lambda_x,\ \lambda_z^{2D} = \lambda_z^{3D} = \lambda_z \text{ and } \lambda_y^{3D} = \lambda_y \tag{17}$$

Using Ababou (1996) expression Eq. (14) in 2D and 3D, and stating that the 2D and 3D components of the effective conductivity should be identical, one gets a system of two equations with two unknowns (K_g^{2D} and σ^2_{Y2D}):

$$K_g^{2D} \exp\left(\sigma^2_{Y2D}\left[\frac{1}{2} - \frac{1}{2}\frac{\lambda_h^{2D}}{\lambda_x}\right]\right) = K_g^{3D} \exp\left(\sigma^2_{Y3D}\left[\frac{1}{2} - \frac{1}{3}\frac{\lambda_h^{3D}}{\lambda_x}\right]\right) \tag{18}$$

and

$$K_g^{2D} \exp\left(\sigma^2_{Y2D}\left[\frac{1}{2} - \frac{1}{2}\frac{\lambda_h^{2D}}{\lambda_z}\right]\right) = K_g^{3D} \exp\left(\sigma^2_{Y3D}\left[\frac{1}{2} - \frac{1}{3}\frac{\lambda_h^{3D}}{\lambda_z}\right]\right) \tag{19}$$

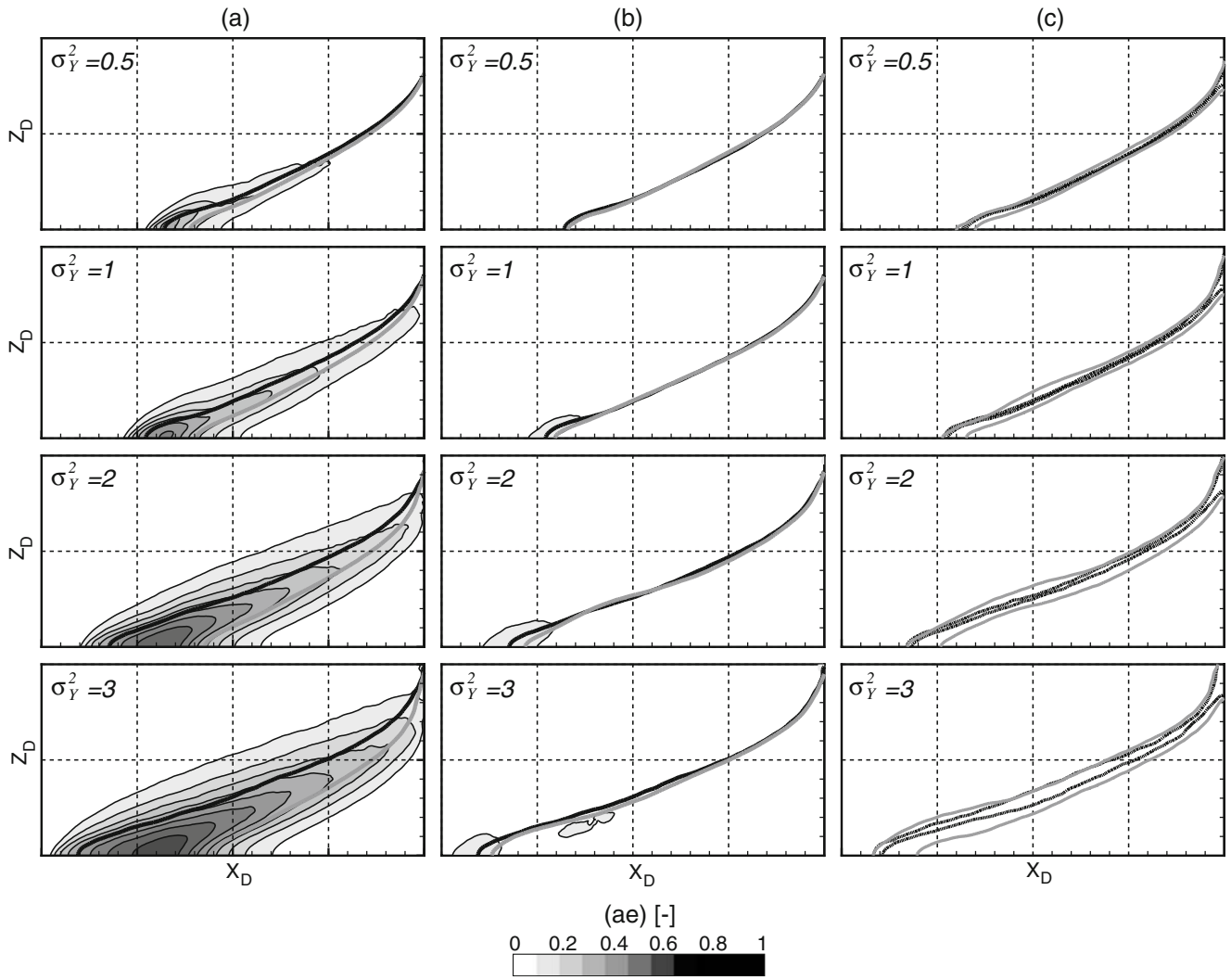

Fig. 11 Comparison between 2D, 2D* and 3D isotropic cases ($l_x = l_y = l_z$=0.04) for different level of *ln(K)* variances. **a** 3D spatial average concentration $C_D^{0.5}$ (*solid black line*), 2D ensemble average concentration $C_D^{0.5}$ before correction (*grey lines*) and the absolute error (ae) in background. Panel **b** is the same as **a** but after transformation of the 2D hydraulic conductivity fields (2D*). **c** 95% confidence interval (mean ± 2 standard deviation) of the relative salt concentration $C_D^{0.5}$ of 3D (*black lines*) and 2D* (*grey lines*)

 DOI 10.1007/s10040-009-0533-0

Table 6 Comparison between 2D and 3D CPU (central processing unit) time requirements

Model configuration	Number of nodes	Seconds of CPU time	Relative CPU time
Two-dimensional	33,153 (257×129)	180	1.00
Three-dimensional	4,276,737 (257×129×129)	135,000	750.00

K_g^{3D} and σ^2_{Y3D} are the known mean and variance of the 3D field. $\lambda_h^{2D}$and λ_h^{3D} are the harmonic means of the correlation lengths in 2D and 3D:

$$\lambda_h^{2D} = \frac{2\lambda_x\lambda_z}{\lambda_x + \lambda_z}, \quad \lambda_h^{3D} = \frac{3\lambda_x\lambda_y\lambda_z}{\lambda_x\lambda_y + \lambda_x\lambda_z + \lambda_y\lambda_z} \tag{20}$$

From Eq. (18), an expression of K_g^{2D} can be obtained and inserted in Eq. (19) to get first the relation between the variance of the 2D field and the one of the 3D field and then an expression of the geometric mean of the 2D field:

$$\sigma^2_{Y2D} = \frac{2}{3}\frac{\lambda_h^{3D}}{\lambda_h^{2D}}\sigma^2_{Y3D} \tag{21}$$

$$K_g^{2D} = K_g^{3D}\exp\left(\sigma^2_{Y3D}\left[\frac{1}{2} - \frac{1}{3}\frac{\lambda_h^{3D}}{\lambda_h^{2D}}\right]\right) \tag{22}$$

In the case of statistically isotropic media $\lambda_h^{2D} = \lambda_h^{3D}$and therefore Eqs. (21) and (22) become:

$$\sigma^2_{Y2D} = \frac{2}{3}\sigma^2_{Y3D} \tag{23}$$

$$K_g^{2D} = K_g^{3D}\exp\left(\frac{\sigma^2_{Y3D}}{6}\right) \tag{24}$$

In summary, if one has an estimation of the correlation lengths in 3D and an estimation of the first two moments of the permeability distribution, assuming a multi-Gaussian distribution one can use Eqs. (21) and (22) to compute the values K_g^{2D} and σ^2_{Y2D} that should be used to model an heterogeneous 2D hydraulic conductivity field having the same effective conductivity than the 3D field. This medium could then be used to investigate in 2D the effect of the 3D heterogeneity. For example one can estimate the uncertainty on the position of the interface for a 3D problem by running many Monte Carlo simulations in 2D, which would be impossible in 3D because of CPU time consideration (Table 6).

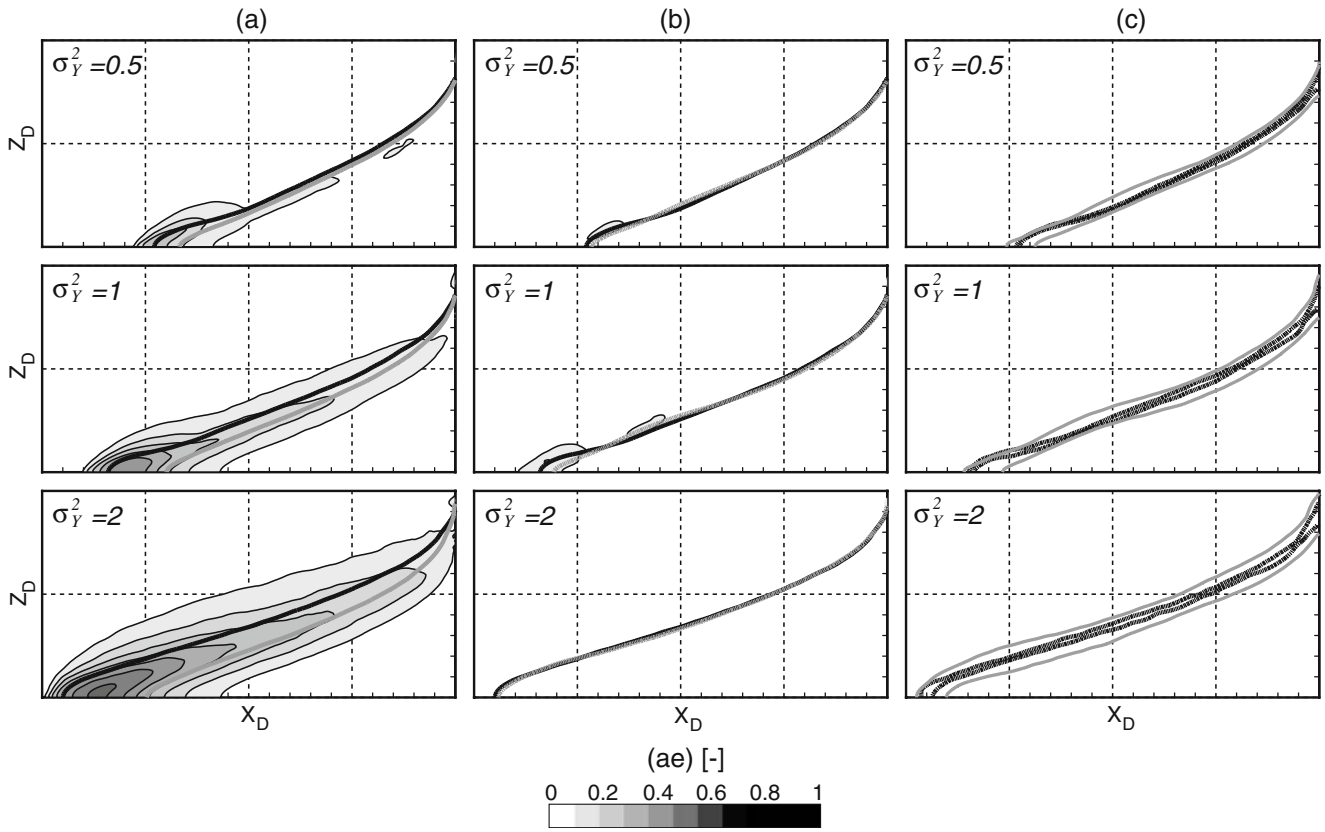

Fig. 12 Comparison between 2D, 2D* and 3D anisotropic cases (l_x=0.12, l_y = l_z=0.04) for different levels of *ln(K)* variances. **a** 3D ensemble spatial average concentration $C_D^{0.5}$ (*solid black line*), 2D ensemble average concentration $C_D^{0.5}$ before correction (*grey lines*) and the absolute error (*ae*) in background. Panel **b** is the same as **a** but after transformation of the 2D hydraulic conductivity filed (2D*). **c** 95% confidence interval (mean ±2 SD) of the relative salt concentration $C_D^{0.5}$ of 3D (*black lines*) and 2D* (*grey lines*)

 DOI 10.1007/s10040-009-0533-0

Numerical test

A numerical evaluation of the proposed approximation was carried out. For each of the cases described earlier in the paper (section Hydraulic conductivity fields), 100 2D simulations were generated with the parameters of the 3D models (K_g^{3D} and σ^2_{Y3D}), and 100 2D* (*: transformed) simulations were generated with the transformed parameters (K_g^{2D} and σ^2_{Y2D}) according to Eqs. (21) and (22). In total, 49 3D hydraulic conductivity fields are compared separately with 49×100 2D simulations.

The comparison is made in terms of absolute error (ae) of the relative concentrations over the whole domain:

$$ae(i,j) = \left| \overline{C_D^{3D}(i,j)} - \overline{C_D^{2D}(i,j)} \right| \tag{25}$$

where i and j are the indices of model cells on the grid, $\overline{C_D^{3D}}$ is the spatial ensemble average in the direction perpendicular to the section on one 3D realization and $\overline{C_D^{2D}}$ is the ensemble average over 100 2D simulations at node (i,j).

The results are in agreement with those obtained in the previous sections. The 2D transformed fields (Figs. 11b and 12b) reproduce much better the mean concentrations computed in 3D than the 2D untransformed fields (Figs. 11a and 12a) for all the values of variances that have been tested. However, the uncertainty on the position of the isoline $C_D^{0.5}$ seems to be systematically slightly larger for the transformed 2D fields than for the 3D models (Figs. 11c and 12c); in any case the 2D estimations of uncertainty on $C_D^{0.5}$ are systematically bounding the 3D ones. Similarly the relative errors on L_D are reduced very significantly when comparing the 2D transformed fields with the 2D original fields (compare Figs. 9 and 13). Before the 2D transformation, the relative error on the saltwater penetration could reach 38% for a variance of 3. By transforming the 2D fields, the error is reduced in general to less than 5%. The width of the mixing is however not better reproduced when considering the transformed fields. It is worth noting that errors due to the ergodicity limitation may partly explain the misfit between 2D* and 3D predictions for larger l_y correlation length (l_y>0.12).

It has been shown in the previous sections (Impact of the heterogeneity and Dimensionality effects) that the differences between 2D and 3D simulations were mainly due to a larger effective hydraulic conductivity in the main flow direction in the 3D models as compared to the 2D ones (both sharing identical statistics of the hydraulic conductivity fields). In addition, more variability of the velocity field in 2D models yielded more dispersion and thus reduced the magnitude of the density driven forces. This results in a shorter toe penetration and larger width of the mixing zone (rotation of the saltwater wedge) in 2D. The proposed transformation reduces the differences between the 2D and the 3D forecasts because not only does it increase the effective hydraulic conductivity in the main flow direction, but it also reduces the variability of a 2D field by reducing its variance.

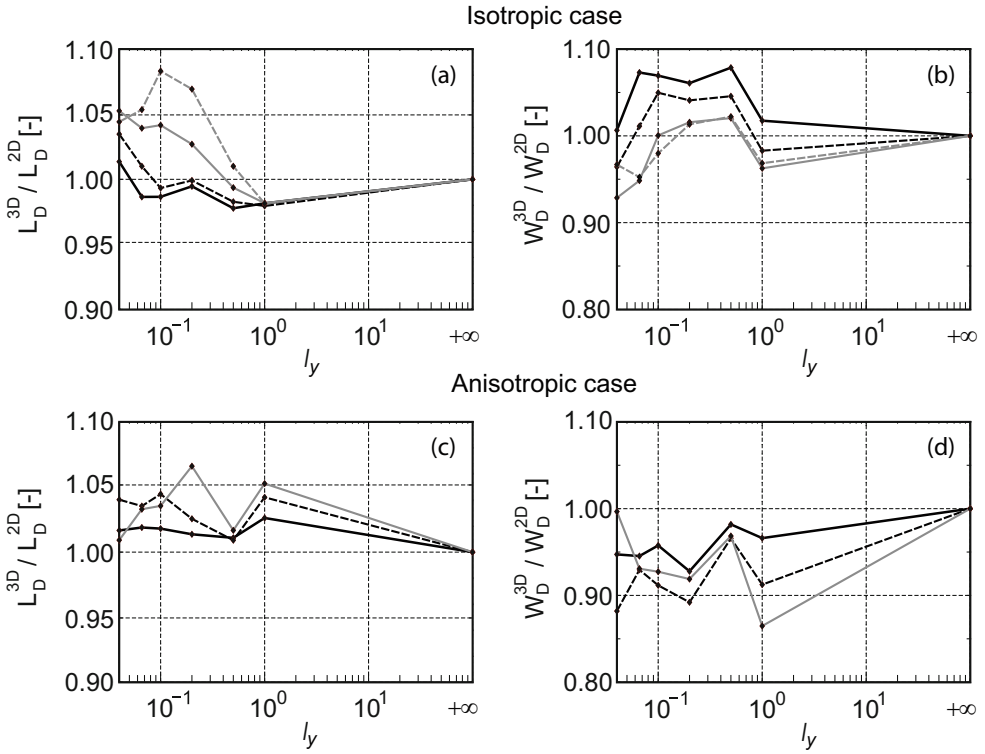

Fig. 13 Dimensionless norms for **a**–**b** the isotropic case and **c**–**d** the anisotropic case. Comparison between 2D* and 3D for different level on *ln(K)* variance (*solid black line* for $\sigma_Y^2 = 0.5$, *dashed black line* for $\sigma_Y^2 = 1$, *solid grey line* for $\sigma_Y^2 = 2$ and *dashed grey line* for $\sigma_Y^2 = 3$)

DOI 10.1007/s10040-009-0533-0

Summary and conclusions

This paper proposes a systematic numerical study of the effects of heterogeneity and dimensionality on seawater intrusion. It shows that the impact of the heterogeneity on seawater intrusion is different in 3D and 2D, both in magnitude and in terms of general trends. For example, when the variance of the log hydraulic conductivity increases, the toe penetration length reduces in 2D, while it may increase or decrease in 3D depending on the degree of heterogeneity and on anisotropy. This is very important because it shows that one cannot extrapolate directly the results of a 2D study to estimate the effect of heterogeneity on a real 3D system. Of course, the numerical experiments were conducted in the framework of a highly idealized system based on an extension of the Henry problem in 3D, but nevertheless this is sufficient to indicate that under a more complex situation involving a nonrectangular geometry and geological heterogeneity, one should also not extrapolate 2D results and be very careful when investigating the possible effects of heterogeneity.

Moreover, the position of the saltwater wedge and the width of the mixing zone can be approximated relatively accurately when the variance is small ($\sigma_Y<1$) with a homogeneous model whose hydraulic conductivity is the equivalent conductivity of the heterogeneous medium computed for a uniform flow through the medium. This is not true for the estimation of the saltwater flux circulating in the seawater wedge, which is always very much higher (between 2 and 20 times higher) in the heterogeneous medium than in the homogeneous medium. When the variance increases, it is not sufficient anymore to use only an equivalent hydraulic conductivity to represent accurately the position of the wedge, the width of the mixing zone or the saltwater flux. This is interpreted as an increased effect of macrodispersion that needs to be accounted for when upscaling the heterogeneous media. This result is in contradiction with the results of Held et al. (2005) who argue that in steady state the macrodispersion has a negligible effect on the saltwater wedge. This difference is certainly due to the fact that the problem that they studied has a very small local dispersivity and is therefore dominated by diffusion, while the work reported here considered higher local dispersivities following the work of Abarca et al. (2007a) because this models a situation that is closer to reality than the initial Henry problem. For the moment, no simple analytical expressions are available to the authors' knowledge to estimate the macrodispersivity under the conditions studied here. It means that one has still to rely on the use of numerical modelling in a heterogeneous domain to analyse the effect of heterogeneity in 2D and in 3D.

When comparing 2D and 3D heterogeneous models, the toe penetration is the parameter most affected by the heterogeneity. The toe position is controlled both in 2D and 3D by the horizontal effective hydraulic conductivity and both by the longitudinal and transversal macro dispersivities, as already shown in 2D by Abarca (2006) and Abarca et al. (2007a). When the effective horizontal hydraulic conductivity increases, the toe penetration length increases. When the macro dispersivity increases, the toe penetration length reduces. These two processes are in competition when the level of heterogeneity increases. Then the dimension of the flow configuration becomes extremely important because the effective hydraulic conductivity or the macro dispersivity evolve differently when increasing the level of heterogeneity in 2D and in 3D. This leads to opposite behaviours in 2D and 3D isotropic media when the level of heterogeneity increases: in 2D the toe penetration length reduces while it increases in 3D. The width of the mixing zone is mainly controlled by dispersion.

In order to facilitate the analysis of 3D cases (which are extremely demanding in terms of computer resources), a technique is proposed to use 2D heterogeneous hydraulic conductivity fields that approximate the 3D saltwater intrusion. The technique consists of generating 2D fields having statistical properties that are different from the real 3D field in such a way that the 2D fields have the right equivalent conductivity tensor. This is achieved by increasing the mean and reducing the variance. This correction is shown to provide a good approximation for the cases that were tested. However, it could certainly be improved further by correcting the longitudinal and transverse dispersivities.

Acknowledgements This work has been funded by the Swiss National Science Foundation under Grants: 207020-110017 and PP002-106557. The authors thank G. de Marsily, R. Ababou, J. Carrera and P. Perrochet for providing valuable suggestions on earlier version of the manuscript as well as Christian Langevin and the anonymous reviewers for their critical but constructive review comments. The authors are also grateful to R. Bouhlila and F. Cornaton for useful discussions about the study.

References

Ababou R (1996) Random porous media flow on large 3D grids: numerics, performance, and application to homogenization, Chap 1, vol 79. In: Wheeler MF (ed) Environmental studies, mathematical, computational & statistical analysis. Springer, New York, pp 1–25

Abarca E (2006) Seawater intrusion in complex geological environments. PhD Thesis, Technical University of Catalonia, Spain

Abarca E, Carrera J, Sánchez-Vila X, Dentz M (2007a) Anisotropic dispersive Henry problem. Adv Water Resour 30:913–926. doi:10.1016/j.advwatres.2006.08.005

Abarca E, Carrera J, Sanchez-Vila X, Voss CI (2007b) Quasi-horizontal circulation cells in 3D seawater intrusion. J Hydrol 339:118–129

Al-Bitar A, Ababou R (2005) Random field approach to seawater intrusion in heterogeneous coastal aquifers: unconditional simulations and statistical analysis. In: Renard P, Demougeot-Renard H, Froidevaux R (eds) Geostatistics for environmental applications. Springer, Heidelberg

Badon-Ghyben W (1888) Nota in verband met de voorgenomen putboring nabij Amsterdam [Notes on the probable results of well drilling near Amsterdam] Tijd Konink Instit Ing 9:8–22

Bear J (1999) Conceptual and mathematical modeling. In: Bear J, Cheng AH-D, Sorek S, Ouazar D, Herrera I (eds) Seawater

intrusion in coastal aquifers: concepts, methods and practices. Kluwer, Dordrecht, The Netherlands, pp 127–161
Bear J (2005) Sea water intrusion into coastal aquifers. In: Anderson M G (ed) Encyclopedia of hydrological sciences. Wiley, Devon, UK
Brovelli A, Mao X, Barry DA (2007) Numerical modeling of tidal influence on density-dependent contaminant transport. Water Resour Res 43, W10426. doi:10.1029/2006WR005173
Burnett RD, Frind EO (1987) Simulation of contaminant transport in 3 dimensions. 2. Dimensionality effects. Water Resour Res 23:695–705
Cornaton F (2007) Ground Water: a 3-D ground water flow and transport finite element simulator. Reference manual, 190 pp. http://www1.unine.ch/chyn/php/softwares.php, October 2009
Croucher AE, O'Sullivan MJ (1995) The Henry problem for seawater intrusion. Water Resour Res 31:1809–1814
Dagan G, Bear J (1968) Solving the problem of local interface upconing in a coastal aquifer by the method of small perturbations. J Hydraul Res 6:15–44
Dagan G, Zeitoun DG (1998) Seawater-freshwater interface in a stratified aquifer of random permeability distribution. J Cont Hydrol 29:185–203
Darvini G, Spendolini L, Salandin P (2002) Saltwater intrusion for finite Peclet numbers in random permeability aquifers. Developments in Water Science. Elsevier, Amsterdam, pp 523–530
Dentz M, Kinzelbach H, Attinger S, Kinzelbach W (2000) Temporal behavior of a solute cloud in a heterogeneous porous medium 1: point-like injection. Water Resour Res 36:3591–3604
Diersch H-JG, Kolditz O (2002) Variable-density flow and transport in porous media: approaches and challenges. Adv Water Resour 25:899–944
Fetter CW (1972) Position of saline water interface beneath oceanic islands. Water Resour Res (5):1307–1315
Gelhar LW (1986) Stochastic subsurface hydrology from theory to applications. Water Resour Res 22:S135–S145
Gelhar LW (1993) Stochastic subsurface hydrology. Prentice-Hall, Upper Saddle River, NJ
Gelhar LW, Axness CL (1983) 3-Dimensional stochastic-analysis of macrodispersion in aquifers. Water Resour Res 19:161–180
Glover RE (1959) The pattern of fresh-water flow in a coastal aquifer. J Geophy Res 64:457–459
Held R, Attinger S, Kinzelbach W (2005) Homogenization and effective parameters for the Henry problem in heterogeneous formations. Water Resour Res 41:1–14. doi:10.1029/2004WR003674
Henry HR (1964) Effects of dispersion on salt encroachment in coastal aquifers. US Geol Surv Water Suppl Pap 1613–C
Herzberg A (1901) Die Wasserversorgung einiger Nordseebader [The water supply of parts of the North Sea coast in Germany]. J Gasbeleucht Verw Beleuchtungsarten Wasserversorg 44:815–819, and 845:824–844
Huyakorn P, Wu YS, Park NS (1996) Multiphase approach to the numerical solution of a sharp interface saltwater intrusion problem. Water Resour Res 32:93–102
Matheron G (1967) Éléments pour une théorie des milieux poreux [Elements for a porous-media theory]. Masson and Cie, Paris
Matheron G (1973) The intrinsic random functions and their applications. Adv Appl Prob 5:439–468
Pohll GM, Warwick JJ, Benson D (2000) On the errors associated with two-dimensional stochastic solute transport models. Trans Porous Med 40:281–293
Reilly TE, Goodman AS (1985) Quantitative-analysis of saltwater fresh-water relationships in groundwater systems: a historical-perspective. J Hydrol 80:125–160
Schwarz C (1999) Dichteabhängige strömungen in homogenen und heterogenen porösen medie [Density-dependent flow in homogenous and heterogeneous porous media]. PhD Thesis, Swiss Federal Institute of Technology, Switzerland
Shapiro AM, Cvetkovic VD (1990) A comparison of 2-dimensional and 3-dimensional stochastic-models of regional solute movement. Trans Porous Med 5:1–25
Simmons CT, Fenstemaker TR, Sharp JM (2001) Variable-density groundwater flow and solute transport in heterogeneous porous media: approaches, resolutions and future challenges. J Cont Hydrol 52:245–275
Simpson MJ, Clement TP (2004) Improving the worthiness of the Henry problem as a benchmark for density-dependent groundwater flow models. Water Resour Res 40, W01504. doi:10.1029/2003WR002199
Strack ODL (1976) Single-potential solution for regional interface problems in coastal aquifers. Water Resour Res 12:1165–1174
Tompson AFB, Ababou R, Gelhar LW (1989) Implementation of the 3-dimensional turning bands random field generator. Water Resour Res 25:2227–2243
Voss CI, Souza WR (1987) Variable density flow and transport simulation of regional aquifers containing a narrow freshwater-saltwater transition zone. Water Resour Res 23:1851–1866
Welty C, Gelhar LW (1991) Stochastic-analysis of the effects of fluid density and viscosity variability on macrodispersion in heterogeneous porous-media. Water Resour Res 27:2061–2075
Welty C, Kane AC, Kauffman LJ (2003) Stochastic analysis of transverse dispersion in density-coupled transport in aquifers. Water Resour Res 39(6):1150. doi:10.1029/2002WR001631